POLITECNICO DI TORINO
Repository ISTITUZIONALE

Eliashberg Analysis of the Electrodynamic Response of Ba(Fe1xRhx)2As2 Across the s± to s++ Order Parameter Transition

(Article begins on next page)

03 May 2024

Eliashberg analysis of the electrodynamic response of Ba(Fe$_{1-x}$Rh$_x$)$_2$As$_2$ across the s$_\pm$ to s$_{++}$ order parameter transition

Daniele Torsello · Giovanni Alberto Ummarino · Roberto Gerbaldo ·
Laura Gozzelino · Gianluca Ghigo

Abstract We report on the Eliashberg analysis of the electrodynamic response of Ba(Fe$_{1-x}$Rh$_x$)$_2$As$_2$ single crystals across the disorder induced $s_\pm$ to s_{++} transition. We previously experimentally identified the transition by its signature in the low temperature value of the penetration depth and observed a peculiar dependency of the critical temperature on disorder; subsequently we proposed new hallmarks in the quasiparticle conductivity and surface impedance. Here we show that this whole set of data can be self consistently reproduced within an effective two-bands Eliashberg model with disorder treated beyond the Born approximation and with a small set of input parameters.

Keywords First keyword · Second keyword · More

1 Introduction

The Eliashberg equations are a powerful and versatile tool to predict and interpret experimentally measured properties of superconductors [1]. Being a generalization of BCS theory, they allow the analysis of materials in which strong coupling effects are relevant, multiband systems and disordered structures. Many physical properties can be calculated and compared to experimental

D. Torsello · R. Gerbaldo · L. Gozzelino · G. Ghigo
Politecnico di Torino, Department of Applied Science and Technology, Torino 10129, Italy
Istituto Nazionale di Fisica Nucleare, Sezione di Torino, Torino 10125, Italy
E-mail: daniele.torsello@polito.it

G. A. Ummarino
Politecnico di Torino, Department of Applied Science and Technology, Torino 10129, Italy
National Research Nuclear University MEPhI (Moscow Engineering Physics Institute), Moskva 115409, Russia

data, giving deep insight in the physics of novel materials [2]. Such an approach was largely employed on the multiband superconductor MgB$_2$, where several properties such as thermal conductivity [3] and surface resistance [4,5], as well as the doping dependence of T_c [6] have been interpreted with the help of Eliashberg models [7].

Iron based superconductors (IBSs) are the most recent example of systems for which BCS theory fails and an Eliashberg approach is necessary to correctly describe their physics [8]. A word of caution should however be used also with respect to Eliashberg approaches if the full superconducting dome needs to be analyzed, because Eliashberg theory is expected to fail near a Lifshitz transition [9]. Such transitions were identified at low electron doping [10] and heavy hole doping [11] in IBSs systems [12]. If we focus on the optimally doped cases, these materials are characterized by the presence of multiple bands that contribute to superconductivity, and electron-boson coupling is provided by antiferromagnetic spin fluctuations [13]. From these properties rises an order parameter that possesses the $s_\pm$ symmetry, i. e. an s-symmetric gap with a π phase shift among different bands [14].

However, experimental proofs of a sign-changing order parameter among different Fermi sheets are difficult to achieve. One possibility is to study the effects of disorder and to observe the signatures of the transition to the sign preserving s_{++} state. Efremov *et al.* showed that at the transition the superfluid density, ρ_s, would increase, corresponding to a dip of the low temperature value of the London penetration depth, $\lambda_L(0)$, as a function of disorder [15]. We previously reported on the first observation of this feature by performing 3.5 MeV proton irradiation on Ba(Fe$_{1-x}$Rh$_x$)$_2$As$_2$ single crystals, measuring $\lambda_L(T)$ with a microwave resonator (MWR) tech-

nique and analyzing this experimental data within an effective two-bands Eliashberg model [16]. The MWR measurements also yields information about the electrodynamic response of the sample [17]. In particular, it was possible to obtain the quasiparticle conductivity, σ_n, and to identify new signatures of the transition [18]. In this paper, we present the Eliashberg analysis of the quasiparticle conductivity across the $s_\pm$ to s_{++} transition, showing that the whole set of experimental data ($\lambda(T)$, T_c and $\sigma_n(T)$ for all levels of disorder) can succesfully be reproduced within an effective two-bands Eliashberg model that suitably takes into account disorder.

Table 1 The table summarizes the values of the parameters used to reproduce the experimental T_c, $\lambda_L(T)$ and $\sigma_n(T)$ of the system after each proton irradiation session, i.e. for different disorder levels, here represented by the average dpa. Γ_1 is the normal state scattering rate that is proportional to disorder, σ is the generalized cross-section, η is the ratio of intra- and inter-band scattering, λ_{ij} are the components of the electron-boson coupling-constant matrix and $w_1=w_1^\sigma=w_1^\lambda$ is the weight of band 1.

dpa ($\times 10^{-3}$)	Γ_1 (meV)	σ	η	λ_{11}	λ_{22}	λ_{12}	w_1
0	0	0	1	1	2.65	-0.17	0.98
1.02	0.361	0	1	1	2.65	-0.17	0.28
3.07	1.08	0.09	1	1	2.65	-0.17	0.25
4.10	1.44	0.10	1	1	2.65	-0.17	0.15
5.12	1.81	0.10	1	1.2	2.65	-0.13	0.90
5.63	1.99	0.14	1	1.2	2.65	-0.13	0.82
6.15	2.17	0.21	1	1.2	2.65	-0.13	0.78
6.63	2.35	0.28	1	1.2	2.65	-0.13	0.75

2 Experimental methods

Optimally doped single crystals of $Ba(Fe_{1-x}Rh_x)_2As_2$ were characterized in the pristine state and for increasing doses of 3.5 MeV proton irradiation using a microwave resonator technique that yields the London penetration depth, quasiparticle conductivity and surface impedance as a function of temperature. All the details of the experimental approach are given elsewhere [19–21,17,1]. The analysis of the penetration depth and superfluid fraction in these samples was reported in [16] and allowed us to identify the $s_\pm$ to s_{++} transition. Moreover, the measured quasiparticle conductivity and surface impedance were discussed in [18] resulting in the identification of two additional signatures of the transition.

3 Eliashberg model

For the purpose of reproducing the experimentally observed features of the London penetration depth and superfluid density and validating the observation of the $s_\pm$ to s_{++} transition, we recently used an effective two-bands Eliashberg model in which disorder was taken into account beyond the Born approximation [16]. The choice of considering two bands instead of a more realistic three- or four- bands model was imposed by the necessity of treating disorder within the T-matrix approach while keeping the number of free parameters reasonable. In order to calculate $\lambda(T)$ and the critical temperature of the system for all levels of disorder, it was sufficient to solve the imaginary-axis version of the Eliashberg equations. By contrast, in the present analysis of the quasiparticle conductivity it is necessary to solve also the equivalent, but numerically more challenging, real-axis Eliashberg equations. The input parameters needed (coupling constants, spectral function, density of states and scattering potential) and the approximations employed are the same as those used in [16] and are summarized in Table 1.

3.1 Real axis equations

In order to calculate the quasiparticle conductivity, one needs the complex frequency dependent gaps $\Delta_i(\omega)$ and renormalization functions $Z_i(\omega)$ on each band i and at all temperatures in the desired range. These can be calculated by solving self-consistently four coupled nonlinear integral equations for these quantities. The real-axis formulation of the Eliashberg equations [22] reads:

$$\Delta_i(\omega,T)Z_i(\omega,T) = \int_0^{\omega_C} d\omega' \Re\left(\frac{\Delta_i(\omega',T)}{\sqrt{\omega'^2 - \Delta_i^2(\omega',T)}}\right) \sum_j \left\{ \int_0^\infty d\Omega \lambda_{ij}\alpha^2 F(\Omega)\right.$$

$$\times \left[(n(\Omega) + f(-\omega'))\left(\frac{1}{\omega + \omega' + \Omega + i\delta^+} - \frac{1}{\omega - \omega' - \Omega + i\delta^+}\right)\right.$$

$$\left.\left. - (n(\Omega) + f(\omega'))\left(\frac{1}{\omega - \omega' + \Omega + i\delta^+} - \frac{1}{\omega + \omega' - \Omega + i\delta^+}\right)\right]\right\}$$

$$+ \sum_j \Gamma_{ij}^N \left(\frac{\Delta_j(\omega,T)}{\sqrt{\omega^2 - \Delta_j^2(\omega,T)}}\right), \tag{1}$$

$$[1 - Z_i(\omega,T)]\omega = \int_0^\infty d\omega' \Re\left(\frac{\omega'}{\sqrt{\omega'^2 - \Delta_i^2(\omega',T)}}\right) \sum_j \left\{ \int_0^\infty d\Omega \lambda_{ij}\alpha^2 F(\Omega)\right.$$

$$\times \left[(n(\Omega) + f(-\omega'))\left(\frac{1}{\omega + \omega' + \Omega + i\delta^+} - \frac{1}{\omega - \omega' - \Omega + i\delta^+}\right)\right.$$

$$\left.\left. - (n(\Omega) + f(\omega'))\left(\frac{1}{\omega - \omega' + \Omega + i\delta^+} - \frac{1}{\omega + \omega' - \Omega + i\delta^+}\right)\right]\right\}$$

$$+ \sum_j \Gamma_{ij}^N \left(\frac{\omega}{\sqrt{\omega^2 - \Delta_j^2(\omega,T)}}\right). \tag{2}$$

Here, ω_C is the boson energy cut-off introduced into the Coulomb repulsion term in order to assure the convergence in (1), $f(\omega) = 1/(e^{\beta\omega} + 1)$ is the Fermi function and $n(\omega) = 1/(e^{\beta\omega} - 1)$ is the Bose function. The real part of the product $\Delta(\omega,T)Z(\omega,T)$ and of $Z(\omega,T)$ is determined by the principal-value integrals in (1) and (2), while the imaginary part comes from the delta-function parts.

The denominators can vanish for particular energies, then the integrals in (1) and (2) must be done carefully when a numerical approach is used.

3.2 Disorder

It is worth underlining that to treat disorder effects as precisely as possible, we implemented a $T-$matrix approach (within an effective two-bands model) that allows us to range from the Born approximation to the unitary limit. Accordingly, we consider both inter-band and intra-band scattering, but it is intended that intra-band terms represent a combination of inter-band terms of a more realistic model that involves all the existing bands.

Γ_{ij}^N in eq.(1) and (2) are the scattering rates from non-magnetic impurities that, in the $T-$matrix model can

be written as:

$$\Gamma_{12(21)}^N =$$
$$= \frac{\Gamma_{1(2)}(1 - \sigma)}{\sigma(1 - \sigma)\eta[N_1(0) + N_2(0)]^2/[N_1(0)N_2(0)] + (\sigma\eta - 1)^2},$$

where $\sigma = \pi^2 N_1(0)N_2(0)u^2/(1 + \pi^2 N_1(0)N_2(0)u^2)$, $\Gamma_{1(2)} = n_{imp}\pi N_{2(1)}(0)u^2(1 - \sigma)$ are the generalized cross-section and normal state scattering rate parameters, respectively, and n_{imp} is the impurity concentration. The parameter η controls the ratio of intra-band and inter-band scattering as $v^2 = u^2\eta$, where v and u are the intraband and interband parts of the impurity potential, respectively [23,24]. When $\sigma \to 0$, disorder is treated within the Born limit (weak scattering), while for $\sigma \to 1$ the unitary limit is achieved (strong scattering). Thus, disorder is controlled by three parameters, namely σ, η and Γ_1, since $\Gamma_2 = \Gamma_1 \frac{N_1(0)}{N_2(0)}$.

The disorder terms in the Eliashberg equations (last line of both eq. (1) and (2)) are obtained for $\eta = 1$ from the more general equations 42 and 43 in [23].

The difference lies in the fact that we assume that the Γ_{ij}^N and $N_j^\Delta(i\omega_n)$ terms can be factorized. This is the same as to say that there is no frequency dependence of the disorder induced scattering. The two expressions are exactly equivalent when $N_1^Z N_2^Z + N_1^\Delta N_2^\Delta \simeq 1$, as it is verified in all our cases [25].
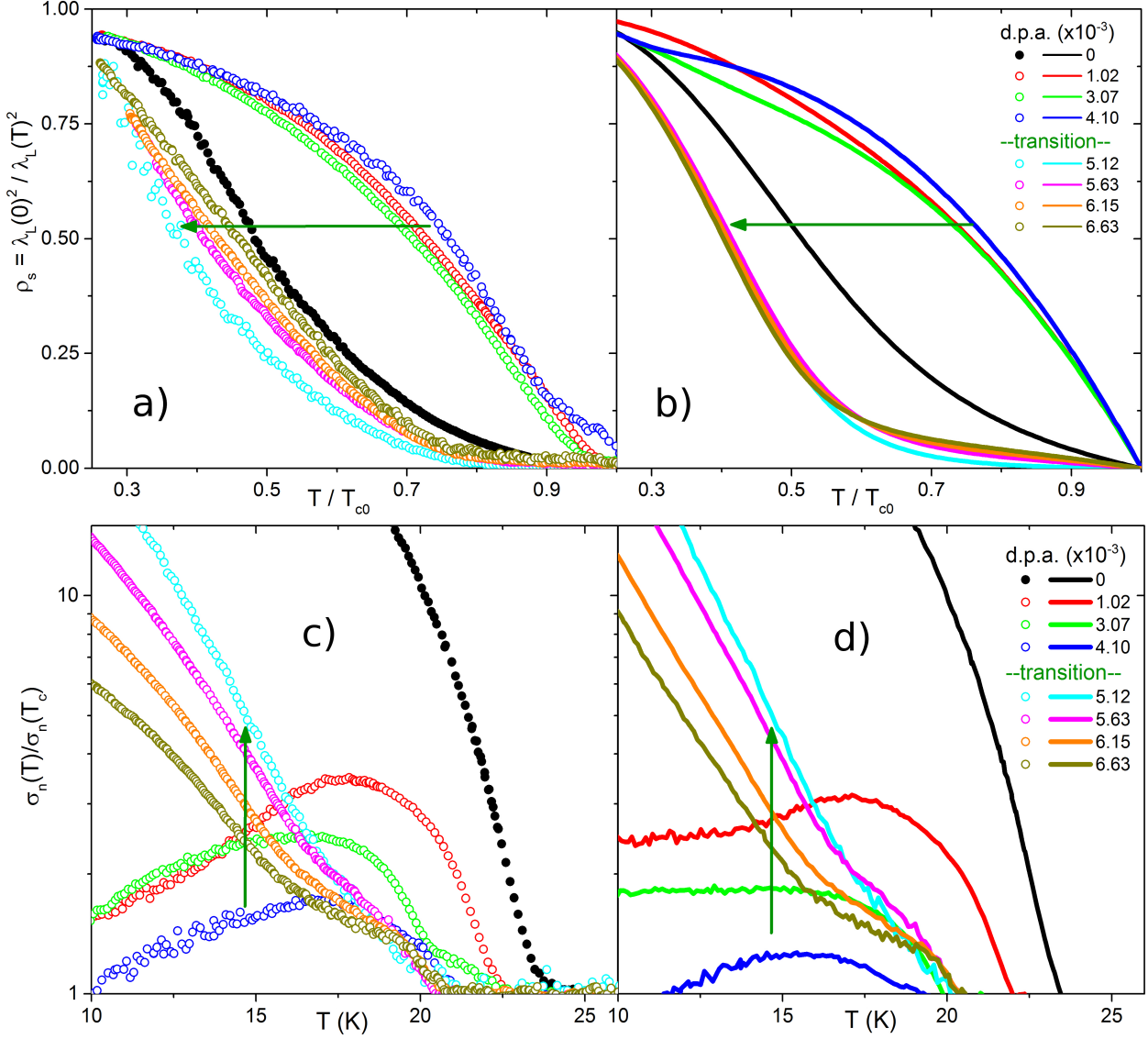
Fig. 1 Comparison between the experimental (left column, symbols) and calculated (right column, solid lines) data of the superfluid fraction (top row) and normalized quasiparticle conductivity (bottom row) for all irradiation doses. Green arrows indicate the changes across the transition.

3.3 Quasiparticle conductivity

The solutions of the Eliashberg equations were then used to determine the microwave conductivity [26]:

$$
\sigma_n(\omega \to 0) = \sum_i w_i^\sigma \sigma_{n,i} =
$$

$$
= \sum_i w_i^\sigma A_i \int_0^{+\infty} d\omega \left(-\frac{\partial f(\omega)}{\partial \omega} \right) \times
$$

$$
\times \left[(\mathrm{Re}\, g_i^Z(\omega))^2 + (\mathrm{Re}\, g_i^\Delta(\omega))^2 \right] \tag{3}
$$

where i is the band index, w_i^σ is the weight of the i-th band (with the constraint that $w_1^\sigma + w_2^\sigma = 1$), and

$$
g_i^Z(\omega) = Z_i(\omega)\omega / \sqrt{[Z_i(\omega)\omega]^2 - [\Delta_i^2(\omega)Z_i^2(\omega)]}
$$

$$
g_i^\Delta(\omega) = \Delta_i(\omega)Z_i(\omega) / \sqrt{[Z_i(\omega)\omega]^2 - [\Delta_i^2(\omega)Z_i^2(\omega)]}
$$

The coefficients A_i depend on the density of states, $N_i(0)$, and on the temperature dependent scattering time, $\tau_i(T)$ of each band. Since these quantities are unknown for these compounds some approximations are necessary: first of all we assume that τ_i has the same temperature dependence for all the bands and therefore we use the effective scattering time obtained from the quantities measured with the MWR technique by means of the phenomenological two-fluid model dis-

cussed in [17].

$$\tau_{TF}^{-1} = \frac{1}{\mu_0 \lambda_L^2(0)\sigma_n} - \frac{\omega(X_s^2 - R_s^2)}{2X_s R_s}. \tag{4}$$

Furthermore, also assuming that the scale factors A_i on different bands are equal ($A_i = A$) and by fitting the conductivities curves normalized to the value at T_c ($\sigma_n(T)/\sigma_n(T_c)$), the weight w_1^σ is left as the only free parameter that can be tuned to reproduce the experimental data. In our case, we use the same weights as those used for the analysis of the penetration depth in [16] (in principle both weights depend on the Fermi velocities on each band), and therefore we have no additional free parameters.

3.4 Results

Figure 1 shows the comparison between the experimental (left column) and calculated (right column) data of the superfluid fraction (top row) and normalized quasiparticle conductivity (bottom row) for all irradiation doses. Despite the approximations employed in the model (the most important of which is the use of a two-band model), the comparison is very satisfactory: all the features are qualitatively and semi-quantitatively reproduced for the whole data set. In particular, it was possible to obtain both monotonous and peaked $\sigma_n(T)$ curves, as the one we observe for different levels of disorder. The combination of experimental and theoretical data (specifically the gap values given in Ref. [16]) allows us to discuss some details about what happens near the disorder driven transition. The observed effects should be interpreted in light of the physical mechanism driving the transition: disorder causes interband scattering that effectively increases mixing between different bands, driving the order parameter values to converge and forcing the smaller one to pass through zero changing its sign [23]. However, it is still unclear whether the transition from $s_\pm$ to s_{++} is a smooth crossover or a discontinuous jump [24, 27, 28]. The gap values obtained with our model (and considering that no experimental data in the range between dpa = 4.10×10^{-3} and 5.12×10^{-3} is available) indicate a quite steep transition, but no distinction is possible between a smooth and a discontinuous transition.

4 Conclusions

In summary, we showed that an effective two-bands Eliashberg model with disorder treated beyond the Born approximation is capable of explaining all the experimentally observed features of the disorder-induced $s_\pm$ to s_{++} transition in a self consistent way, with only a few free parameters. In particular, it was possible to reproduce the experimental normalized quasiparticle conductivity as a function of temperature for all levels of disorder across the transition with no additional free parameter with respect to those optimized for the superfluid density.

References

1. D. Torsello, G.A. Ummarino, L. Gozzelino, T. Tamegai, G. Ghigo, Phys. Rev. B **99**, 134518 (2019). DOI 10.1103/PhysRevB.99.134518. URL https://link.aps.org/doi/10.1103/PhysRevB.99.134518
2. G.A. Ummarino, D. Daghero, M. Tortello, R.S. Gonnelli, Journal of Superconductivity and Novel Magnetism **24**(1), 247 (2011). DOI 10.1007/s10948-010-1006-3. URL https://doi.org/10.1007/s10948-010-1006-3
3. E. Bauer, C. Paul, S. Berger, S. Majumdar, H. Michor, M. Giovannini, A. Saccone, A. Bianconi, Journal of Physics: Condensed Matter **13**(22), L487 (2001). DOI 10.1088/0953-8984/13/22/107. URL https://doi.org/10.1088%2F0953-8984%2F13%2F22%2F107
4. G. Ghigo, D. Botta, A. Chiodoni, L. Gozzelino, R. Gerbaldo, F. Laviano, E. Mezzetti, E. Monticone, C. Portesi, Phys. Rev. B **71**, 214522 (2005). DOI 10.1103/PhysRevB.71.214522. URL https://link.aps.org/doi/10.1103/PhysRevB.71.214522
5. G. Ghigo, G.A. Ummarino, R. Gerbaldo, L. Gozzelino, F. Laviano, E. Mezzetti, Phys. Rev. B **74**, 184518 (2006). DOI 10.1103/PhysRevB.74.184518. URL https://link.aps.org/doi/10.1103/PhysRevB.74.184518
6. S. Agrestini, C. Metallo, M. Filippi, L. Simonelli, G. Campi, C. Sanipoli, E. Liarokapis, S. De Negri, M. Giovannini, A. Saccone, A. Latini, A. Bianconi, Phys. Rev. B **70**, 134514 (2004). DOI 10.1103/PhysRevB.70.134514. URL https://link.aps.org/doi/10.1103/PhysRevB.70.134514
7. G. Ummarino, R. Gonnelli, S. Massidda, A. Bianconi, Physica C: Superconductivity **407**(3), 121 (2004). DOI https://doi.org/10.1016/j.physc.2004.05.009
8. O.V. Dolgov, I.I. Mazin, D. Parker, A.A. Golubov, Phys. Rev. B **79**, 060502 (2009). DOI 10.1103/PhysRevB.79.060502. URL https://link.aps.org/doi/10.1103/PhysRevB.79.060502
9. D. Innocenti, S. Caprara, N. Poccia, A. Ricci, A. Valletta, A. Bianconi, Superconductor Science and Technology **24**(1), 015012 (2010). DOI 10.1088/0953-2048/24/1/015012. URL https://doi.org/10.1088%2F0953-2048%2F24%2F1%2F015012

10. C. Liu, T. Kondo, R.M. Fernandes, A.D. Palczewski, E.D. Mun, N. Ni, A.N. Thaler, A. Bostwick, E. Rotenberg, J. Schmalian, et al., Nature Physics **6**(6), 419 (2010)
11. N. Xu, P. Richard, X. Shi, A. van Roekeghem, T. Qian, E. Razzoli, E. Rienks, G.F. Chen, E. Ieki, K. Nakayama, T. Sato, T. Takahashi, M. Shi, H. Ding, Phys. Rev. B **88**, 220508 (2013). DOI 10.1103/PhysRevB.88.220508. URL https://link.aps.org/doi/10.1103/PhysRevB.88.220508
12. A. Bianconi, Nature Physics **9**(9), 536 (2013)
13. D. Inosov, J. Park, P. Bourges, D. Sun, Y. Sidis, A. Schneidewind, K. Hradil, D. Haug, C. Lin, B. Keimer, V. Hinkov, Nature Physics **6**(3), 178 (2010)
14. I.I. Mazin, D.J. Singh, M.D. Johannes, M.H. Du, Phys. Rev. Lett. **101**(5), 057003 (2008). DOI 10.1103/physrevlett.101.057003. URL https://doi.org/10.1103%2Fphysrevlett.101.057003
15. D.V. Efremov, M.M. Korshunov, O.V. Dolgov, A.A. Golubov, P.J. Hirschfeld, Phys. Rev. B **84**(18), 180512(R) (2011). DOI 10.1103/physrevb.84.180512. URL https://doi.org/10.1103%2Fphysrevb.84.180512
16. G. Ghigo, D. Torsello, G.A. Ummarino, L. Gozzelino, M.A. Tanatar, R. Prozorov, P.C. Canfield, Phys. Rev. Lett. **121**, 107001 (2018). DOI 10.1103/PhysRevLett.121.107001. URL https://link.aps.org/doi/10.1103/PhysRevLett.121.107001
17. G. Ghigo, D. Torsello, R. Gerbaldo, L. Gozzelino, F. Laviano, T. Tamegai, Supercond. Sci. Technol. **31**(3), 034006 (2018). DOI 10.1088/1361-6668/aaa858
18. D. Torsello, R. Gerbaldo, L. Gozzelino, M.A. Tanatar, R. Prozorov, P.C. Canfield, G. Ghigo, The European Physical Journal Special Topics **228**(3), 719 (2019). DOI 10.1140/epjst/e2019-800144-1. URL https://doi.org/10.1140/epjst/e2019-800144-1
19. G. Ghigo, G.A. Ummarino, L. Gozzelino, T. Tamegai, Phys. Rev. B **96**(1), 014501 (2017). DOI 10.1103/PhysRevB.96.014501. URL http://link.aps.org/doi/10.1103/PhysRevB.96.014501
20. G. Ghigo, G.A. Ummarino, L. Gozzelino, R. Gerbaldo, F. Laviano, D. Torsello, T. Tamegai, Sci. Rep. **7**(1), 13029 (2017). DOI 10.1038/s41598-017-13303-5. URL http://www.nature.com/articles/s41598-017-13303-5
21. D. Torsello, K. Cho, K.R. Joshi, S. Ghimire, G.A. Ummarino, N.M. Nusran, M.A. Tanatar, W.R. Meier, M. Xu, S.L. Bud'ko, P.C. Canfield, G. Ghigo, R. Prozorov, Phys. Rev. B **100**, 094513 (2019). DOI 10.1103/PhysRevB.100.094513. URL https://link.aps.org/doi/10.1103/PhysRevB.100.094513
22. J.P. Carbotte, Rev. Mod. Phys. **62**, 1027 (1990). DOI 10.1103/RevModPhys.62.1027. URL https://link.aps.org/doi/10.1103/RevModPhys.62.1027
23. M.M. Korshunov, Y.N. Togushova, O.V. Dolgov, Physics-Uspekhi **59**(12), 1211 (2016). URL http://stacks.iop.org/1063-7869/59/i=12/a=1211
24. V.A. Shestakov, M.M. Korshunov, Y.N. Togushova, D.V. Efremov, O.V. Dolgov, Supercond. Sci. Technol. **31**(3), 034001 (2018). URL http://stacks.iop.org/0953-2048/31/i=3/a=034001
25. Here $N_j^{\Delta}(i\omega_m) = \Delta_j(i\omega_m)/\sqrt{\omega_m^2 + \Delta_j^2(i\omega_m)}$ and $N_j^Z(i\omega_m) = \omega_m/\sqrt{\omega_m^2 + \Delta_j^2(i\omega_m)}$
26. O.V. Dolgov, A.A. Golubov, D. Parker, New Journal of Physics **11**(7), 075012 (2009). URL http://stacks.iop.org/1367-2630/11/i=7/a=075012
27. H. Kontani, S. Onari, Phys. Rev. Lett. **104**, 157001 (2010). DOI 10.1103/PhysRevLett.104.157001. URL https://link.aps.org/doi/10.1103/PhysRevLett.104.157001
28. V. Shestakov, M. Korshunov, O. Dolgov, Symmetry **10**(8), 323 (2018)